Hyperfine Interactions **144/145:** 45–52, 2002.

Recent Developments in Synchrotron Mössbauer Reflectometry

L. DEÁK[1], L. BOTTYÁN[1], M. MAJOR[1], D. L. NAGY[1], H. SPIERING[2], E. SZILÁGYI[1] and F. TANCZIKÓ[1]
[1]*KFKI Research Institute for Particle and Nuclear Physics, Budapest, Hungary*
[2]*Institute für Anorganische und Analytische Chemie, Johannes Gutenberg Universität, Mainz, Germany*

Abstract. Synchrotron Mössbauer Reflectometry (SMR), the grazing incidence nuclear resonant scattering of synchrotron radiation, can be applied to perform depth-selective phase analysis and to determine the isotopic and magnetic structure of thin films and multilayers. Principles and methodological aspects of SMR are briefly reviewed. Off-specular SMR provides information from the lateral structure of multilayers. In anti-ferromagneticly coupled systems the size of magnetic domains can be measured.

Key words: Mössbauer reflectometry, magnetic multilayers, off-specular scattering, antiferromagnetic domains, anisotropic optics.

1. Introduction

Although features of nuclear resonant scattering (NRS) of thin films were realized and dealt with from the early 60s [1], it has only been recently that the high brilliance and high degree of polarization of synchrotron radiation (SR), monochromator and detector techniques at 3rd generation sources allowed NRS to develop into a spectroscopic method in surface and thin film magnetism. For brevity, we call NRS of SR on thin films Synchrotron Mössbauer Reflectometry (SMR). SMR combines the sensitivity of Mössbauer spectroscopy to hyperfine interactions with the depth information yielded by reflectometry. SMR is established in the time and angular regime. Time differential (TD) SMR gives local (beating due to hyperfine interaction) information at a given incidence angle, time integral (TI) SMR gives an integral hyperfine interaction depth profile and superstructure information. Off-specular scattering and incoherent scattering offer novel applications.

The general description of specular reflection of grazing incidence Mössbauer radiation was given by Hannon *et al.* [2–5]. Starting from the quantum theory of γ-radiation, they formulated the dynamic theory of Mössbauer optics. Unfortunately, the dynamic theory provides rather slow algorithms for calculating reflectivity spectra; therefore, it is less efficient in spectrum fitting. In the grazing incidence limit, an optical model was derived from the dynamical theory [3, 5], which has

been implemented in numerical calculations [6]. As it was shown later [7], this optical method is equivalent to that of Ref. [8].

The rigorous derivation of the general formulae for the transmissivity and the reflectivity of γ-radiation in the forward scattering and the grazing incidence case, respectively, were given by Deák *et al*. [8]. Like in Refs. [9–12], the Afanas'ev–Kagan nucleon current density expression of the dielectric tensor [13] and the covariant anisotropic optical formalism [14] were used. Instead of calculating the susceptibility tensor χ from the current densities of the nucleons, however, the problem was reduced to the calculation of the coherent forward scattering amplitude f. In the case of forward scattering, this general approach led to the theory of Blume and Kistner [15]. Using no intuitive pre-assumptions, Ref. [8] represents a firm basis of the Blume–Kistner theory [15] and of the Andreeva approximation [9–12]. The obtained reflectivity formulae in [8] are also suitable for fast numerical calculations in order to actually *fit* the experimental data [7].

The first successful grazing incidence NRS experiment with SR was performed by Grote *et al.* [16] in 1991. Chumakov *et al*. observed a pure nuclear reflection of SR from an isotopically periodic ^{57}Fe/Sc/^{56}Fe/Sc multilayer [17]. Alp *et al.* reported on the observation of nuclear resonant specular reflection with ^{119}Sn resonance [18]. An important step towards the realization of SMR was the observation of the *total reflection peak* [19, 20], i.e. the high number of *delayed* photons appearing close to the critical angle of the *electronic* reflectivity. The first SMR experiment aiming at the study of the magnetic structure of an anti-ferromagnetic (AF) ^{57}Fe/Cr multilayer was done by Toellner *et al*. [21]. The last years saw an increasing number of SMR experiments as a standard method for studying multilayers and thin films [22, 23].

2. Principles of specular SMR

In NRS of SR the low-lying levels of an ensemble of identical nuclei are coherently excited by the synchrotron radiation pulse. Since the levels are, as a rule, split by hyperfine interactions, the spatial and temporal coherence of the scattering results in characteristic patterns both of the angular distribution and the time evolution of the scattered radiation, which bear simultaneous and correlated information about topology and internal fields in the sample under study. SR is scattered both by nuclei and by electrons and these two processes interfere with each other, as well. Conventional Mössbauer spectroscopy and NRS of SR, although delivering similar information on hyperfine interaction and lattice dynamics, are complementary rather than equivalent to each other. The principal difference is that when the energy spectrum is scanned by the Doppler-shifted radiation of a γ-source, the recorded signal presents the incoherent sum of the spectral components of the transmitted radiation. In case of time domain NRS of SR, however, the response is formed by the coherent sum of the spectral components of the scattered radiation.

The specular SMR measurement is performed in θ–2θ geometry, in either time integral (TISMR) or time differential regime (TDSMR). TISMR means recording the total number of delayed photons from t_1 to t_2 as a function of θ. The time t_1 is a few nanoseconds and is determined by the bunch quality of the radiation source and by the dead time of the detector and the electronics, t_2 is a value somewhat below the bunch repetition time of the storage ring. As a rule, a θ–2θ scan of the *prompt* photons (conventionally called X-ray reflectometry) is recorded along with a delayed time integral SMR scan. TDSMR is a time response measurement in a fixed θ–2θ geometry performed at different values of θ. Like in the forward scattering case, hyperfine interaction results in quantum beats of the time response. The first step of an SMR measurement is usually to take a TISMR scan to select θ values of high enough delayed count rates at which TDSMR measurements can be performed. These regions are found near the total reflection peak [19, 20] and, in case of electronic or nuclear periodicity, near the electronic or nuclear Bragg reflections. A full SMR measurement consists of a prompt, a delayed time integral specular reflectivity scan, and a set of time response reflectivity measurements of the delayed photons. To extract the depth profile of hyperfine interactions with confidence, all these data should be evaluated *simultaneously*. If a full SMR measurement is not feasible for intensity reasons, a TISMR scan may still contain valuable information on the structure of the thin film.

Giving qualitative picture from the method we show a simple example on Figure 1, the simulation of a hypothetical two-dimensional energy-domain reflectivity spectrum of $[^{57}\text{Fe}(3.0\text{ nm})/^{56}\text{Fe}(1.5\text{ nm})]_{10}$ isotope periodical multilayer on glass as substrate.

Mössbauer reflectometry (MR) is a unification of reflectometry and Mössbauer spectroscopy. Indeed, taking the cross-sections at a fixed energies E on Figure 1, we get reflectometry spectra, as shown on Figure 2. For the given energies E having the index of reflection n from the expression of Lax [24] and using the op-

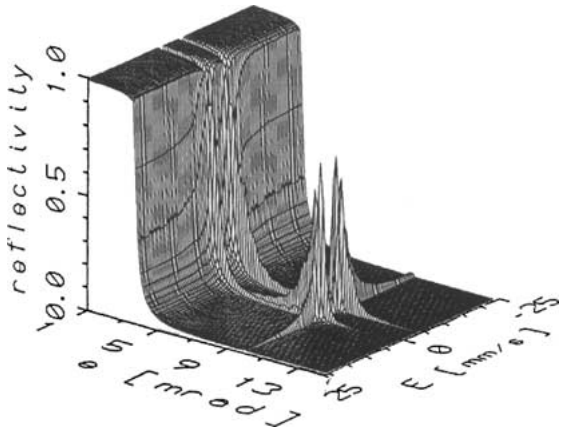

Figure 1. Energy-domain reflectivity of $^{57}\text{Fe}/^{56}\text{Fe}$ multilayer.

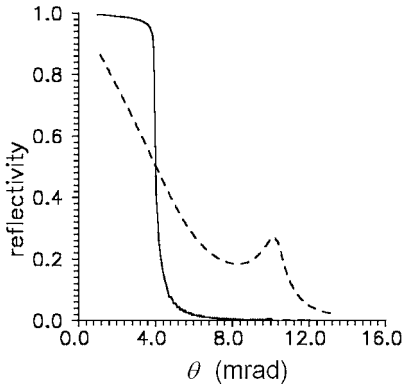

Figure 2. Reflectivity curves at resonance ($E = 3.072$ mm/s, dashed line) and off resonance at $E =$ 25 mm/s (solid line).

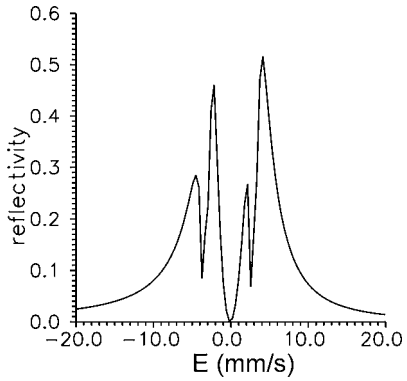

Figure 3. Mössbauer spectrum at the Bragg position ($\theta = 10.123$ mrad).

tical picture [6, 8], reflectometry spectra can be calculated as generalized Fresnel-formulae [6, 8]. Because of the isotopic periodicity we have a Bragg-peak at $\theta =$ 10.123 mrad on Figures 1 and 2 for energies near the resonance. However, far from the resonances, only the electronic scattering has considerable probability, so the spectrum is the X-ray reflectivity curve. From point of view of electronic scattering, the isotopic structure does not give any contrast, and the Bragg-peak disappears. On the other hand, taking the cross-sections at fixed grazing angles θ we get the energy dependent Mössbauer spectra (Figure 3). In the model, the hyperfine field was parallel to the surface of the multilayer and transversal electric, *viz.* σ-polarized, incident beam was assumed. In this special case there are only two Mössbauer lines at $E = \pm 3.072$ mm/s. The broadening and asymmetry of the individual lines are caused by the multiple scattering and the strong dispersion near the nuclear resonance; furthermore the asymmetry between the lines are caused by the electronic scattering.

Using SR as source, the simultaneous broadband coherent excitation results in time-domain SMR spectra, those are the Fourier-transformed reflectivity curves

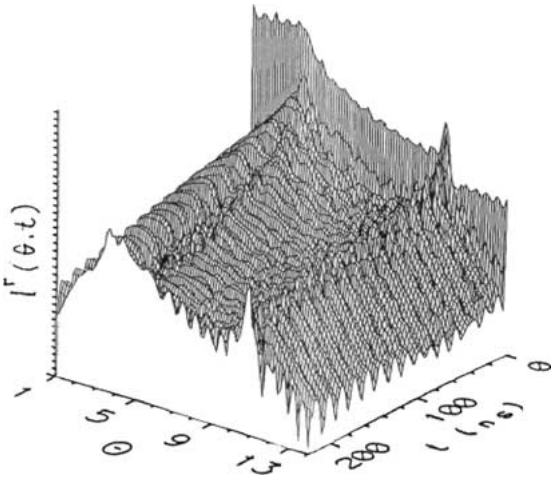

Figure 4. Time-domain reflectivity spectrum of ^{57}Fe/^{56}Fe multilayer.

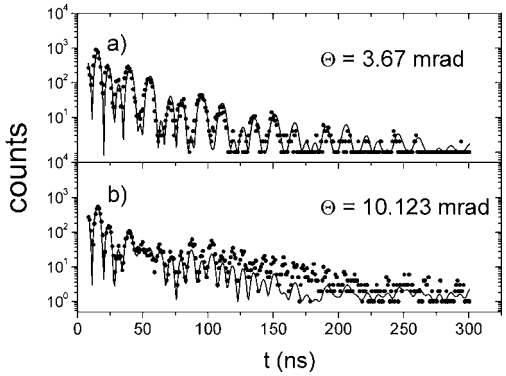

Figure 5. Experimental and theoretical TDSMR spectra of an ^{57}Fe/^{56}Fe multilayer at $\theta = 3.67$ mrad (near the critical angle) (a) and at $\theta = 10.123$ mrad (Bragg position) (b).

of the complex energy-domain, as shown on Figure 4. The TDSMR spectra, we measure (Figure 5), are the cross-sections at a fixed grazing angle θ of the two-dimensional surface in Figure 4. TISMR means integration of the TDSMR spectra from t_1 to t_2 as a function of θ, where t_1 and t_2 define fix time interval (Figure 6), as it was explained in the previous paragraph.

On the TISMR spectrum (Figure 6) we also see the Bragg peak ($\theta = 9$ mrad) [25] and an additional peak at the critical angle, $\theta = 3.67$ mrad, this latter being the interference effect of the electronic and nuclear scattering of photons [19, 20]. There is no Bragg peak on the X-ray reflectivity curve (Figure 6), as it was explained earlier.

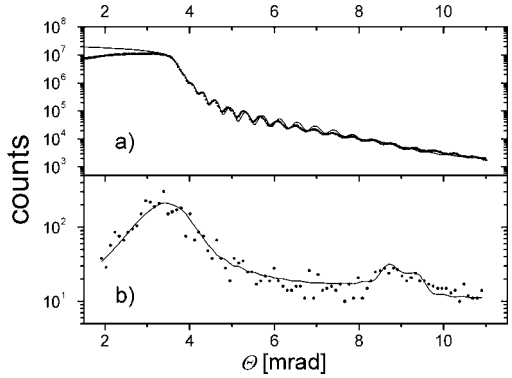

Figure 6. Non-resonant X-ray reflectivity (a) and TISMR (b) spectra of an ^{57}Fe/^{56}Fe multilayer.

3. Off-specular SMR

The specularly reflected radiation from layered systems does not depend on the lateral structure; it depends only on the lateral averages of material parameters [24, 26]. For studying lateral inhomogeneities, such as magnetic domains, etc., one can apply off-specular reflectometry. One possibility for off-specular reflectometry is the geometry called "ω-scan", where we fix the value of 2Θ (i.e. the detector) and vary the sample orientation ω (leaving the constraint of specular reflection $\omega = \Theta$).

Starting from the general theory of Lax [24] the off-specular intensity I_{off} can be expressed by the Fourier transformed depth profile of the coherent field inside the layers $T(\mathbf{k}'_\perp)$ ($\mathbf{k}'_\perp$ is the perpendicular component of the momentum of the scattered wave) and by the lateral Fourier transformation of the autocorrelation function of susceptibilities $C(\mathbf{K}_{\text{II}})$ ($\mathbf{K}_{\text{II}}$ being the later component of the momentum transfer vector)

$$I_{\text{off}} \propto \text{Tr}\left\lfloor T^{+}\left(\mathbf{k}'_\perp\right) C(\mathbf{K}_{\text{II}}) T\left(\mathbf{k}'_\perp\right) \rho \right\rfloor,$$

where ρ is the polarization density matrix of the incident radiation [27]. As 0th approximation we may assume that the autocorrelation function is exponential and so $I_{\text{off}} \propto C(\mathbf{K}_{\text{II}})$ is Lorentzian [27]. It follows that the correlation length is inversely proportional to the widths of the Lorentzian.

Figure 7 shows the off-specular X-ray reflectometry ("prompt") and off-specular SMR ("delayed") measurements on MgO(001)[^{57}Fe(26 Å)/Cr(13 Å)]$_{20}$ AF multilayer at the AF-Bragg position. The X-ray ω-scan resulted in a narrow line, indicating that there were no structural inhomogeneities in the lateral direction, additionally the wide Lorentzian on the delayed ω-scan shows the lateral inhomogeneity in the hyperfine magnetic field as a result of the magnetic domains. From the Lorentzian fit (solid line in Figure 7) we get 0.8 μm average domain size.

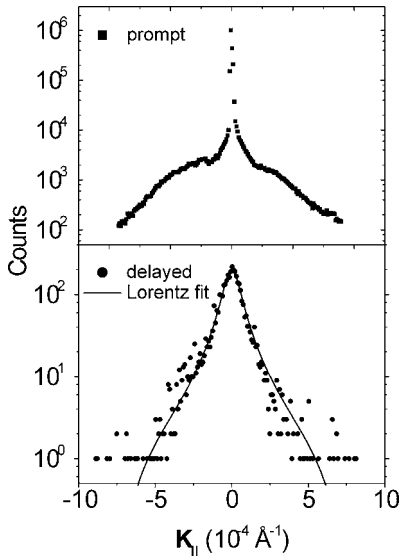

Figure 7. Prompt and delayed off-specular scans on MgO(001)[^{57}Fe(26 Å)/Cr(13 Å)]$_{20}$ AF multilayer at the AF-Bragg position. The solid line shows the Lorentzian fit.

4. Conclusion

A short overview of specular and off-specular SMR was given. Off-specular SMR is sensitive to the lateral structure of the hyperfine fields, so it can be used for studying magnetic domains in multilayers. Using the method we found 0.8 μm average domain size in a MgO(001)[^{57}Fe(26 Å)/Cr(13 Å)]$_{20}$ AF multilayer. The off-specular data evaluation will be soon available in EFFI (Environment For FItting).

Because of the underlying common optical approach the same theory can be applied for SMR, X-ray reflectometry, spin polarized neutron reflectometry [26] and X-ray resonance exchange scattering [28, 29] for both specular and off-specular reflexion. The computer program EFFI based on this calculus is freely available [7, 30].

Acknowledgements

This work was partly supported by the Hungarian Scientific Research Fund (OTKA) under Contract No. T029409 and by the Hungarian Academy of Sciences (Contact No. AKP 97-104 2,2/17). The financial support by the Deutsche Forschungsgemeinschaft (DFG) is gratefully acknowledged. The access to SR was generously made possible by ESRF Grenoble and HASYLAB Hamburg.

References

1. Bernstein, S. and Campbell, E. C., *Phys. Rev.* **132** (1963), 1625.
2. Hannon, J. P. and Trammell, G. T., *Phys. Rev.* **169** (1968), 315.
3. Hannon, J. P. and Trammell, G. T., *Phys. Rev.* **186** (1969), 306.
4. Hannon, J. P., Hung, N. V., Trammell, G. T., Gerdau, E., Mueller, M., Rüffer, R. and Winkler, H., *Phys. Rev. B* **32** (1984), 5068.
5. Hannon, J. P., Trammell, G. T., Mueller, M., Gerdau, E., Rüffer, R. and Winkler, H., *Phys. Rev. B* **32** (1985), 6363.
6. Röhlsberger, R., Ph.D. thesis, University Hamburg, 1994.
7. Spiering, H., Deák, L. and Bottyán, L., *Hyp. Interact.* **125** (2000), 197.
8. Deák, L., Bottyán, L., Nagy, D. L. and Spiering, H., *Phys. Rev. B.* **53** (1996), 6158.
9. Irkaev, S. M., Andreeva, M. A., Semenov, V. G., Beloserskii, G. N. and Grishin, O. V., *Nucl. Instrum. Methods B* **74** (1993), 554.
10. Andreeva, M. A., Irkaev, S. M. and Semenov, V. G., *Sov. Phys. JETP* **78** (1994), 965.
11. Andreeva, M. A. and Kuz'min, R. N., *Messbauerovskaya Gamma-Optika*, Moscow University, 1982.
12. Andreeva, M. A. and Rosete, K., *Poverkhnost'* **9** (1986), 145; *Vestnik Mosk. Univ.*, *Ser. 3. Fiz. Astron.* **27** (1986), 57.
13. Afanas'ev, A. M. and Kagan, Yu., *Sov. Phys. JETP* **21** (1965), 215.
14. Borzdov, G. M., Barskovskii, L. M. and Lavrukovich, V. I., *Zh. Prikl. Spektrosk.* **25** (1976), 526.
15. Blume, M. and Kistner, O. C., *Phys. Rev.* **171** (1968), 417.
16. Grote, M., Röhlsberger, R., Dimer, M., Gerdau, E., Hellmich, R., Hollatz, R., Jäschke, J., Lüken, E., Metge, J., Rüffer, R., Rüter, H. D., Sturhahn, W., Witthoff, E., Harsdorff, M., Pfützner, W., Chambers, M. and Hannon, J.-P., *Europhys. Lett.* **14** (1991), 707.
17. Chumakov, A. I., Smirnov, G. V., Baron, A. Q. R., Arthur, J., Brown, D. E., Ruby, S. L., Brown, G. S. and Salashchenko, N. N., *Phys. Rev. Lett.* **71** (1993), 2489.
18. Alp, E. E., Mooney, T. M., Toellner, T., Sturhahn, W., Witthoff, E., Röhlsberger, R., Gerdau, E., Homma, H. and Kentjana, M., *Phys. Rev. Lett.* **70** (1993), 3351.
19. Baron, A. Q. R., Arthur, J., Ruby, S. L., Chumakov, A. I., Smirnov, G. V. and Brown, G. S., *Phys. Rev. B* **50** (1994), 10354.
20. Deák, L., Bottyán, L. and Nagy, D. L., *Hyp. Interact.* **92** (1994), 1083.
21. Toellner, T. L., Sturhahn, W., Röhlsberger, R., Alp, E. E., Sowers, C. H. and Fullerton, E. E., *Phys. Rev. Lett.* **74** (1995), 3475.
22. Chumakov, A. I., Nagy, D. L., Niesen, L., Alp, E. E., *Hyp. Interact.* **123/124** (1999), 427.
23. Röhlsberger, R., *Hyp. Interact.*, **123/124** (1999), 455.
24. Lax, M., *Rev. Mod. Phys.* **23** (1951), 287.
25. The Bragg position is different, because the model system differs by this measurement and simulation. The sample was: float glass/^{57}Fe(4.6 nm)/[^{56}Fe(2.9 nm)/^{57}Fe(2.3 nm)]□15/Al(5.7 nm).
26. Deák, L., Bottyán, L., Nagy, D. L. and Spiering, H., *Physica B* **297** (2001), 113.
27. Deák, L., to be published.
28. Hannon, J. P., Trammell, G. T., Blume, M. and Doon Gibs, *Phys. Rev. Lett.* **61** (1988), 1245.
29. Deák, L. *et al.*, to be published (not yet implemented into our data evaluation program, EFFI).
30. The computer program EFFI is available from ftp://iacgu7.chemie.uni-mainz.de/pub/effi.